MULTI-SPACECRAFT STUDIES IN AID OF SPACE WEATHER SPECIFICATION AND UNDERSTANDING

V. Angelopoulos[1], M. Temerin[1], I. Roth[1], F. S. Mozer[1], D. Weimer[2], and M. R. Hairston[3]

[1]*Space Sciences Laboratory, University of California, Berkeley, CA, USA*
[2]*Mission Research Corporation, Nashua, NH, USA*
[3]*W. B. Hanson Center for Space Sciences, University of Texas, Dallas, TX, USA*

ABSTRACT

We present particle modeling in prescribed magnetic and electric fields during the February 17-18, 1998 magnetic storm in an effort to explain observed ion signatures on three spacecraft (POLAR, EQUATOR-S and FAST) which sampled the inner magnetosphere over a wide range of L-shells. The objective is to improve global electric field models, which are crucial to the evolution of the storm-time particle distributions. We back-trace ion distributions from the satellite locations and keep track of charge-exchange losses. The electric field models used are the Volland-Stern, Weimer 96, Weimer 2000 and a version of the Weimer 96 model modified to best fit instantaneous potential measurements made by the electric field instrument on POLAR and the ion drift meter instrument on DMSP satellites. We find that the Weimer 2000 model provides the best agreement with the data. However differences with observations do exist and cannot be accounted for simply by modification of existing models. Explaining those differences requires addition of either nightside injections or global storm-time inductive electric fields.

MOTIVATION

The global electric field distribution in the magnetosphere is a far more elusive quantity than the global magnetic topology. Normally low altitude satellites have been used to obtain the spacecraft potential and model it. Assuming the field lines are equipotentials (an approximation valid only when the allowable uncertainty can be larger than the typical field aligned potential drop of a few kV) the global electric field can then be obtained. Such efforts since the early days of multiple balloon (Mozer et al., 1974) and low altitude satellites (e.g., S3-3) have led to an increasingly improved understanding of the global ionospheric electric field patterns (Heelis et al., 1982). Semi-empirical models like the Volland-Stern model, hereby referred to as the “VS” model, (Volland, 1973; Stern, 1975) started to develop; they were quickly compared and fitted against data under arbitrary activity conditions (Maynard and Chen, 1975). More recently, the availability of the DE and the DMSP datasets has led to more sophisticated models of the average electric potential pattern under a variety of solar wind conditions (Heppner and Maynard, 1987; Rich and Hairston, 1994). A spherical harmonic representation of the fits to the electric potential averages of DE by Weimer (1996) has led to a generalized data-based model, herein termed the “W96” model, which can compute the ionospheric potential pattern under any interplanetary magnetic field orientation. This model was recently enhanced to the “W2k” model, to include the effects of nightside convection increases under substorm conditions using the AL index as an activity proxy (Weimer, 2001). All models above have been derived from large statistical databases and thus cannot proclaim to represent accurately storm time electric fields. In fact, recent evidence from

CRESS (Wygant et al., 1998) suggests that such fields penetrate to much lower latitudes than during non-storm periods. The low latitude electric fields probably play a key role in populating the innermost L-shells, but neither their origin nor their effects have been adequately understood because of the lack of electric field measurements in the equatorial inner magnetosphere.

Efforts to understand particle evolution during substorms and storms have been remarkably successful in reproducing gross features of particle distributions in the inner magnetosphere, using the aforementioned simple electric field models and the assumption that the field lines are equipotentials. Specifically, Ejiri et al. (1980) were able to model nose dispersions, one of the most dramatic features of substorm and storm time fluxes at the inner magnetosphere at dusk (Smith and Hoffman, 1974), using a step function for the electric field increase in a dipole field. “Nose” refers to the shape of the dispersion of a particle enhancement seen in a energy versus L-shell spectrogram, predominantly at dusk. Only particles of energy ~10-20 keV make it to low L-shells because under a steady electric field those energies correspond to open trajectories and are constantly replenished with particles from the tail. Lower energies correspond to EXB-dominated closed trajectories and higher energies correspond to gradient/curvature drift-dominated closed trajectories, both inaccessible by tail ions. The long residence in closed trajectories allows losses (such as charge-exchange) to deplete ions of those energies.

The effect of an ion lifetime limited in comparison to the residence time on a drift path was invoked to explain another feature of ion spectra, such as a decrease of flux at a discrete energy around a few keV seen in energy-time spectrograms of satellites in the inner magnetosphere (McIlwain, 1972). The ions which are lost at discrete energies are a subset of the ions with open trajectories (accessible from the tail), but simply take a long time to arrive at the satellite location. The energy of lost particles signifies the transition from EXB-dominated to gradient/curvature drift-dominated orbits. This principle was used by Kistler et al. (1989), Fok et al. (1996) and Jordanova et al. (1999) to explain observed storm time ion spectra on single satellite passes. Charge exchange is the dominant loss process. Kistler et al. (1999) compared the particle fluxes obtained from backtracing bounce averaged particle orbits in a dipole magnetic field and time-dependent models of the electric field. They used the VS and the W96 global electric field models whose time-dependence was obtained from the time dependence of the Kp index (for the VS model) or the solar wind parameters (for the W96 model). The resultant fluxes were compared against storm-recovery phase observations by the EQUATOR-S satellite, with the objective to ascertain the electric field model that results in best agreement with the data. The authors found that the W96 model does a better job in reproducing the spectral features of the ions, but that neither model can accurately predict the energies of the observed minima.

In this work we extend the analysis of Kistler et al. (1999) on the February 17-18 1998 storm, by incorporating the POLAR and FAST satellite observations to our analysis and by using additionally a modified W96 electric field model and the W2k model. Details on the storm evolution can be found in that paper. Our objectives are: 1) to see how the existing picture for a storm studied by one inner magnetospheric spacecraft (EQUATOR-S) changes from the inclusion of data from two other spacecraft, and 2) to test the capability of two new electric field models to reproduce the observed particle features.

TRACING PROCEDURE

We used a guiding center model of the particle motion in a prescribed electric and a dipole magnetic field. The VS and W96 models reproduce the same results as those of Kistler et al. (1999) but for small differences which may be attributed to the exact implementation of the time dependence of the electric field model (interpolation/averaging procedure of Kp and of solar wind input). We start at a given time and a given satellite's dipole latitude and longitude. We backtrace ions which at are locally mirroring at the satellite location (though our guiding center code can study any other pitch angle). Backtracing lasts for 24 hours, or until the ions reach an L-shell of 10. We assume ions are protons. At each time we keep track of the ratio of the instantaneous particle phase space density to the one at the satellite, by updating the particle losses due to charge exchange. This is done, like in Kistler et al. (1999), by using the neutral geocoronal model of Rairden et al. (1986) and the charge-exchange cross section for protons tabulated in Smith and Bewtra (1978). If backtracing stops at L=10 (open orbit) the source phase space density is obtained from a Maxwellian of T=20 keV and N=0.1 cm^{-3}. If backtracing stops at 24hours (closed orbit) then the source distribution (at L<10) was also derived from a Maxwellian with the same properties as at L>10, but assuming adiabatic transport to the backtracing stopping point. Other distributions consistent with FAST storm-time statistical averages, or with CCE typical observations (Kistler et al., 1989) were attempted with similar results. The specifics of our choice of an initial distribution on closed trajectories affects only the depth of the spectral minima, not their position. Our choice of the initial distribution on open trajectories does affect the final particle spectra. The specific choice of temperature and density reflects a visual best match to the data.

ELECTRIC FIELD MODELS

Analytical expressions from dipole mapping were used to obtain the electric field at any given location from the electric field at the ionosphere as specified by the VS, W96 and W2k models. We implemented the VS model by obtaining the 3-hour Kp index, re-sampling on 1 hour intervals and then computing the electric field at the position of each particle after linearly interpolating to obtain the instantaneous Kp value. The solar wind values to input in the W96 and W2k models were obtained from 10 minute averages in the WIND database projected forward in time to correspond to their values at Earth. The data (IMF By, Bz, Vsw and Nsw) were linearly interpolated at the times of interest before they entered the W96 or W2k model. Similarly, the AL index (provisional) was obtained at 1min resolution from the World Data Center and interpolated at the times of interest before usage by the W2k model.

The modified W96 model (herein referred-to as "W96mod" model) represents an attempt to improve the instantaneous electric field model using available measurements of the polar cap potential by the DMSP and POLAR satellites. The idea is that even though the electric field models may not be accurate representations of the global electric field distribution during storms, they can get closer to reality once their input parameters are "tweaked" such that the results match observed traces of the polar cap potential. To that end we used one POLAR pass over the southern oval (at 0610-0850 UT on Feb. 18) and integrated the electric field measured by the EFI instrument [Harvey et al., 1995] along the spacecraft velocity vector to produce the potential along the orbit, assuming the potential is zero at low latitudes (<55^{o}). After subtracting the corotation potential, a small potential difference was found between the two 55° latitude points at the two legs of the oval pass (inbound and outbound). The difference was assumed to be due to a small temporal change of the polar cap potential over the ~2.5 hr period of the pass. As such it was subtracted from the trace of the potential, by linearly interpolating in time from zero to the full value. In addition to the POLAR data we used data from four DMSP satellites (F11, F12, F13 and F14). The ion drift meter on those satellites provides the ion velocity components perpendicular to the spacecraft motion, which are then used to obtain the potential along the spacecraft track, assuming that the potential is zero at low latitudes. Here too the corotation potential was subtracted and the potential offset between the opposite low latitude points on each pass were assumed to be due to temporal variations and were subtracted after linear interpolation in time.

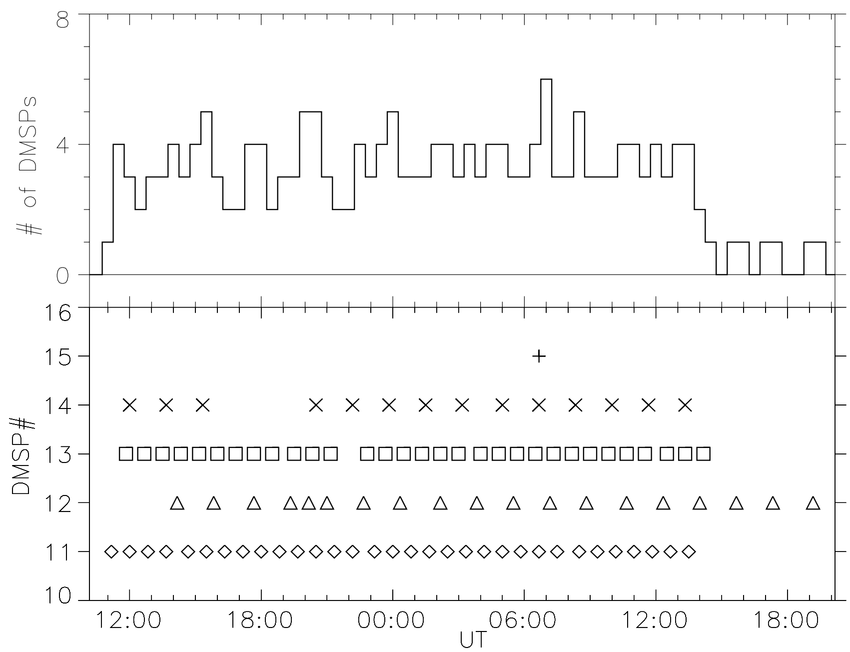

Fig. 1. Bottom: Satellite oval crossings available arranged by satellite. The number denotes DMSP number, except for #15, which denotes POLAR. Number of available passes within 2-hour intervals centered on 1/2 hour centers.

Figure 1 (bottom) shows the center times of each oval pass by the POLAR and the four DMSP satellites. The top figure shows the number of oval crosses during a sliding two hour period centered on half hour centers (anywhere from 2-6 satellite passes available each time). For these multiple crosses we obtained the value of the W96 potential starting from the average solar wind conditions during the given 2 hour interval and then varied the input parameters (By, Bz and Vsw) so as to minimize the difference with the observed potential. All passes were mostly in a dawn-dusk fashion at various distances from the terminator (depending on dipole tilt), providing a relatively good measure of the full potential drop. The resultant parameters for a best fit to the data varied significantly from the initial solar wind parameters, and mostly in a manner that tended to decrease the total W96 potential drop. This is in agreement with the conclusion of Weimer (2001) that the W96 model overestimates the transpolar cap potential drop during storms. This procedure provides a new set of W96 model input parameters at a half hour resolution, which we linearly interpolate in time to obtain instantaneous values of the electric field at the time and position of interest for particle orbit integrations. The above constitutes our “W96mod” model.

PARTICLE DATA

In addition to EQUATOR-S, two more satellites equipped with thermal plasma instrumentation crossed a large range of L-shells during the recovery phase of the February 17-18, 1998 storm. These were POLAR and FAST. Information on ion (assumed proton) spectra is obtained on POLAR from the HYDRA instrument (Scudder et al., 1995) and on FAST from the ion electrostatic analyzer instrument (Carlson et al., 2001). The energy-time spectrograms of the energy flux seen on the three spacecraft, along with their positions are shown at the bottom three panels on Figure 2.

As explained in Kistler et al. (1999) EQUATOR-S was at the prenoon sector and observed at least two energy minima (one at ~10 keV and another at a few keV) inside of L~7. It is evident in the spectrogram that the average energy of both main minima decreases as L-shell decreases.

POLAR, in the postnoon sector, observed one main minimum at ~10 keV. The minimum increased in energy as the satellite moved to smaller L-shells and attained its maximum energy at the innermost L-shell (8:20 UT). The energy of the minimum decreased thereafter as POLAR moved to the northern hemisphere at higher L-shells. A second minimum is observed at ~9:30 UT at energies of ~15 keV and its energy decreases with time (i.e., L-shell). This minimum might have been present at higher energies at earlier times but would be beyond the energy range of the instrument. Other minima at lower energies are also present but are not as clear at 90^{o} pitch angles. They are much clearly defined at the spectrograms of field-aligned (or field-opposed) particles (not shown). Such lower energy-dispersed ion features have been seen also by Freja and other satellites (e.g., Yamauchi et al., 1996) and can be interpreted as nightside injections (Ebihara et al., 2001).

FAST, in the prenoon sector was approaching the polar cusp when it also observed a major flux minimum at ~ 10 keV, between 1110 and 1116 UT. Lower energy enhancements (<1keV) are also interpreted as injections. At 11:16 UT FAST reached the regions adjacent to the cusp and at 1118 UT it entered the cusp, as evidenced by the enhancement of magnetosheath-like (~1keV) plasma population.

RESULTS

We use the aforementioned electric field models (VS, W96, W96mod and W2k) to trace particle orbits in a dipole field and compute, assuming charge-exchange losses, the particle spectrograms at three satellite locations (EQUATOR-S, POLAR and FAST). The results are shown in Figure 2, along with (and in the same format as) the data to which we are comparing our results.

All electric field models do an adequate job in predicting the fluxes seen on FAST. Specifically the 10 keV minimum is reproduced by all electric field models. This is due to ions which spend much time in the inner magnetosphere because their EXB eastward drift is roughly balanced by their westward gradient/curvature drift. The sharp change in the character of the model energy fluxes is due to the motion of FAST poleward of L=10, which results in immediate assignment of a phase space density consistent with a 20 keV, 0.1cm^{-3} Maxwellian to those points. In reality, the FAST data show a hot magnetospheric-like population prior to entry to the cusp. This layer of hot plasma is thought to come from the tail (Newell and Meng, 1992) due to distortions of the dipole mapping which cannot be accounted for in our model.

On POLAR, the modeled fluxes depend significantly on the electric field model chosen. The VS field produces a broad and deep minimum. The W96 model produces more moderate (and realistic losses) while both the W96mod and the W2k models produce a double minimum. The energy of both minima has the correct trend in terms of L-shell dependence (peak energy at lowest L-shell). However, the minima are at different energies relative to the observed values.

On EQUATOR-S, all models result in a principal minimum at around 10keV in agreement with the principal minimum observed in the data. The W96 model has a broad minimum, which generally is a poorer reproduction of the observed fluxes (not clearly distinguished in the energy flux spectrogram format). The W2k models result in a robust secondary minimum at around 20 keV. This secondary minimum is not very clear in the energy flux spectrogram but it is clearly seen in the spectra of percent particle loss due to charge-exchange in Figure 3. The position of the two minima does not agree well with the observations. In addition, the L-shell dependence of the position of the minima is contrary to what is seen in the data: While in the data both minima decrease in energy with decreasing L-shell, all our models show an increase in the energy of the minima with decreasing L-shell.

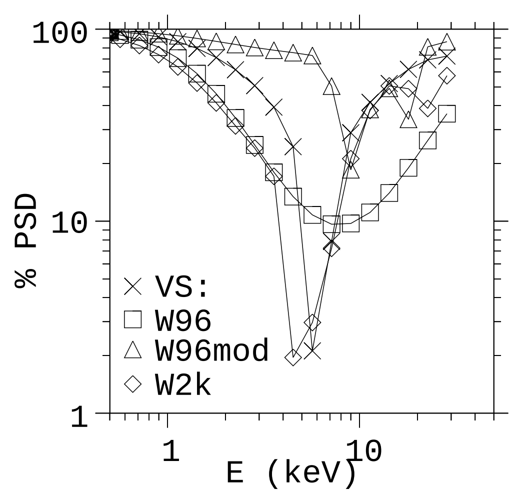

Fig. 3 Spectra of % of ions left after losses by charge exchange. Secondary minima at ~20 keV are evident on spectra derived using W96mod and W2k models.

The L-shell dependence of the energy of the minima is understood in the following fashion: The energy minimum represents the energy where the curvature/gradient drift balances the EXB drift. A decrease in L-shell (which in a dipole field results in a decrease in curvature/gradient drift) requires a higher particle energy in order to balance the same EXB drift. This is a behavior relatively independent of electric field model used. The data however shows a decrease in energy with decreasing L-shell. Assuming that the gradient/curvature drifts are modelled accurately enough, this observation suggests that the real EXB drift decreases with decreasing L-shell faster than any model would predict. This is in agreement with the observation of Wygant et al. (1998) of reverse sign, intense fields in the inner magnetosphere during storms. Since the storm data-based W96mod model also shows the same behavior as the other models in terms of L-shell dependence of the location of the minimum, we conclude that low altitude observations of electric fields are not sufficient to monitor the high altitude electric field in the magnetosphere. Since low L-shells are being considered, the most likely explanation for the discrepancy is the presence of intense inductive electric fields which are expected to be present during storms.

An alternative explanation of the energy spectrograms may be that indeed the primary ion population exhibits a primary minimum increasing in energy with decreasing L-shell, but superimposed on the spectrogram is the signature of two injections with energy decreasing as a function of L-shell. The two injections start at energies of 5 and 10 keV at 9:30 UT and end at energies 1 and 3 keV respectively. Modelling of this alternative interpretation of the data would require time dependent and localized (inductive) electric field enhancement(s) at the nightside. Similar work (e.g., Li et al., 2000) has shown promise that it can explain single satellite spectrograms. If applied in this case it would have to be consistent with observations on other satellites as well. The above two scenaria are beyond the scope of this paper.

ACKNOWLEDGMENTS

We wish to thank C. W. Carlson for making the FAST data available and J. Scudder for making the POLAR/HYDRA data available for this study. We are grateful to L. Kistler for useful discussions. This work was supported under NASA contract NAS5-30367.

REFERENCES

Carlson, C. W., et al., The electron and ion plasma experiment for FAST, Space Sci. Rev., in press (2001).

Ebihara, Y., et al., Wedge-like dispersion of sub-keV ions in the dayside magnetosphere: Particle simulation and Viking observations, J. Geophys. Res., in press (2001).

Ejiri, M., et al., Energetic particle penetrations into the inner magnetosphere, J. Geophys. Res., 85, 653 (1980).

Fok, M.-C., et al., Ring current development during storm main phase, J. Geophys. Res., 101, 15311, (1996).

Fok, M.-C., and T. E. Moore, Ring current modeling in a realistic magnetic field configuration, Geophys. Res. Lett., 24, 1775 (1997).

Harvey, P., et al, The electric field instrument on the POLAR satellite, Space Sci. Rev., 71, 583, 1995.

Heelis, R. A., et al., A model of the high-latitude ionospheric convection pattern, J. Geophys. Res., 87, 6339 (1982).

Heppner, J. P., and N. C. Maynard, Empirical high-latitude electric field models, J. Geophys. Res., 92, 4467 (1987).

Jordanova, V. K., et al., Simulations of off-equatorial ring current ion spectra measured by Polar for a moderate storm at solar minimum, J. Geophys. Res., 104, 429, (1999).

Kistler, L. M., et al., Energy spectra of the major ion species in the ring current during geomagnetic storms, J. Geophys. Res., 94, 3579 (1989).

Kistler, L. M., et al., Testing electric field models using ring current ion energy spectra from the Equator-S ion composition (ESIC) instrument, Ann. Geophysicae, 17, 1611 (1999).

Li, X., et al., Multiple discrete-energy ion features in the inner magnetosphere: Observations and simulations, Geophys. Res. Lett., 27, 1447 (2000).

Maynard, N. C. and A. J. Chen, Isolated cold plasma regions: observations and their relation to possible production mechanisms, J. Geophys. Res., 80, 1009 (1975).
McIlwain, C. E., Plasma convection in the vicinity of the geosynchronous orbit, in Proceedings of a Symposium on Earth's magnetospheric processes, edited by McCormak, B. M. Dordrecht, Netherlands, D. Reidel Publishing Co, p. 268 (1972).
Mozer, F.S., et al., High-latitude electric fields and the three-dimensional interaction between the interplanetary and terrestrial magnetic fields, J. Geophys. Res., 79, 56 (1974).
Newell, P. T. and C. I. Meng, Mapping the dayside ionosphere to the magnetosphere according to particle precipitation characteristics, Geophys. Res. Lett., 19, 609 (1992).
Rairden, R. L., et al., Geocoronal imaging with Dynamics Explorer, J. Geophys. Res., 91, 13613 (1986).
Rich, F. J., and M. Hairston, Large-scale convection patterns observed by DMSP, J. Geophys. Res., 99, 3827 (1994).
Scudder, J., et al., HYDRA - a 3-dimensional electron and ion hot plasma instrument for the POLAR spacecraft of the GGS mission, Space Sci. Rev., 71, 459 (1995).
Smith, P. H., and R. A. Hoffman, Direct observations in the dusk hours of the characteristics of the storm time ring current particles during the beginning of magnetic storms, J. Geophys. Res., 79, 966 (1974).
Smith, P. H., and N. K. Bewtra, Charge exchange lifetimes for ring current ions, Space Sci. Rev., 22, 301 (1978).
Stern, D. P., The motion of a proton in the equatorial magnetosphere, J. Geophys. Res., 80, 595 (1975).
Volland, H., A semi empirical model of large-scale magnetospheric electric fields, J. Geophys. Res., 78, 171 (1973).
Weimer, D. R. A flexible IMF dependent model of high-latitude electric potentials having "space weather" applications, Geophys. Res. Lett., 23, 2549 (1996).
Weimer, D. R., An improved model of ionospheric electric potentials including substorm perturbations and application to the Geospace Environment Modeling November 24, 1996, event, J. Geophys. Res., 106, 407 (2001).
Wygant, J., et al., Experimental evidence on the role of the large spatial electric field in creating the ring current, J. Geophys. Res., 103, 29527 (1998).
Yamauchi, M., et al., Meso-scale structures of radiation belt/ring current detected by low-energy ions, Adv. Space Sci., 17, 171 (1996).

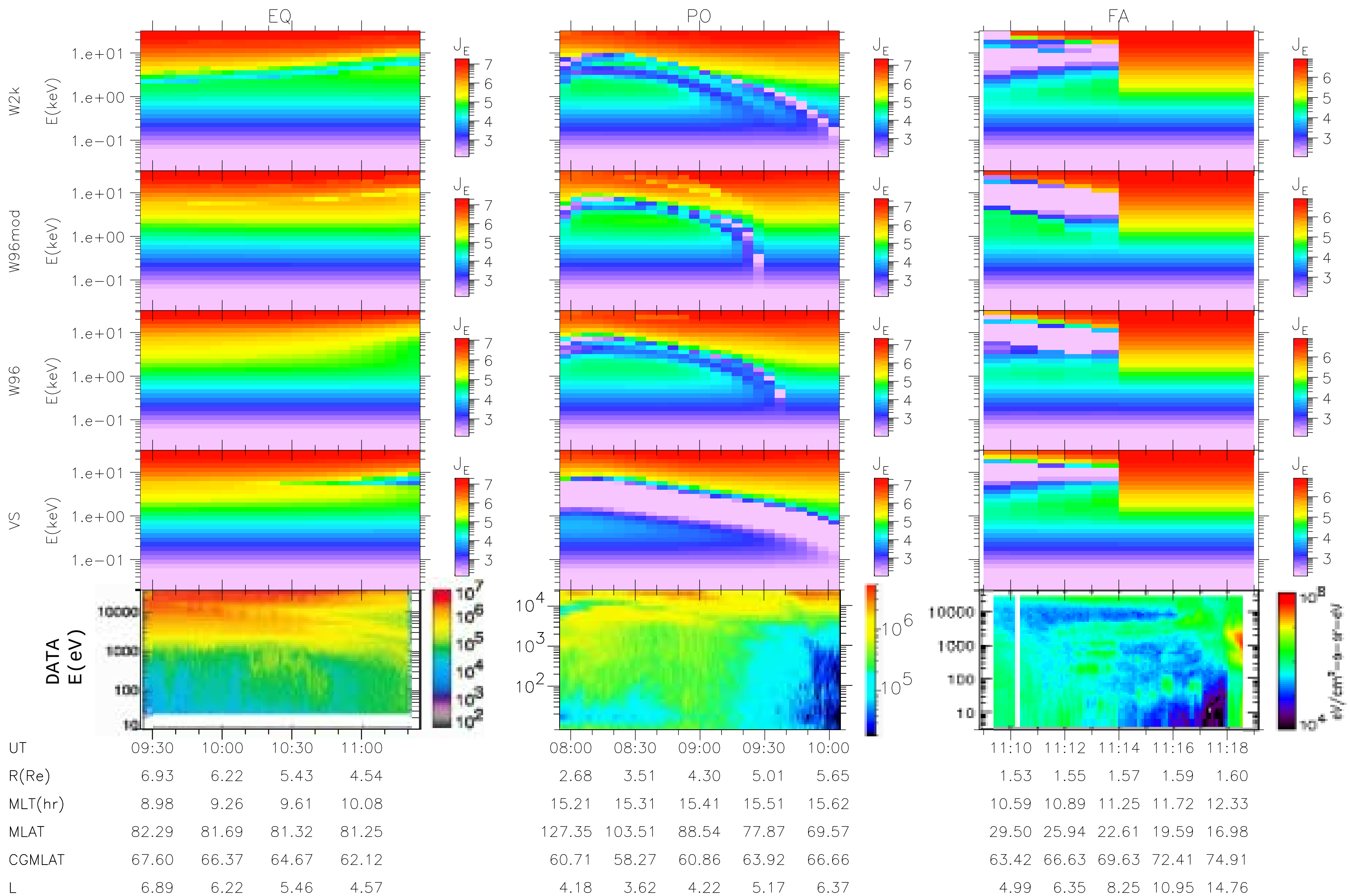

Fig. 2 Data (bottom panels) and model-derived (other panels) energy flux spectrograms from three satellites (EQUATOR-S, left panels; POLAR: middle panels; FAST: right panels). The electric field model used (same on each row) is indicated on the left.